DOI: 10.1021/ma900817t

Macromolecules
ARTICLE

Relation between Photoactive Layer Thickness, 3D Morphology, and Device Performance in P3HT/PCBM Bulk-Heterojunction Solar Cells

Svetlana van Bavel,[†,§] Erwan Sourty,[†,⊥] Gijsbertus de With,[†] Kai Frolic,[†] and Joachim Loos*[,†,§,‡]

[†]*Laboratory of Materials and Interface Chemistry and Soft-Matter CryoTEM Research Unit,* [‡]*Laboratory of Polymer Technology, Eindhoven University of Technology, P.O. Box 513, NL-5600 MB Eindhoven, The Netherlands,* [§]*Dutch Polymer Institute, Eindhoven University of Technology, P.O. Box 902, NL-5600 AX Eindhoven, The Netherlands, and* [⊥]*FEI Company, Achtseweg Noord 5, Building AAE, NL-5600 KA Eindhoven/Acht, The Netherlands*

Received April 15, 2009; Revised Manuscript Received August 19, 2009

ABSTRACT: To get an efficient organic solar cell, as much light as possible should be absorbed by the photoactive layer; as a consequence, thick layers should be preferable. However, it is often observed that much thinner photoactive layers result in more efficient devices than the corresponding thicker layers absorbing more light. Besides light absorption, other aspects such as efficient exciton dissociation, charge transportation, and charge collection are of crucial importance, and all of them are strongly influenced by the volume morphology of the photoactive layer. In this study of bulk-heterojunction solar cells based on poly(3-hexylthiophene) (P3HT) and a methanofullerene derivative (PCBM), we show that the resulting P3HT/PCBM morphology is strongly determined by the layer thickness because the kinetics of solvent evaporation and crystallization is different in films of different thickness. For the preparation conditions chosen in this study, an optimum morphological organization of the photoactive layer characterized by high crystallinity of P3HT, viz. numerous crystalline P3HT nanowires forming a genuine three-dimensional network, and enrichment of crystalline P3HT closer to the hole collecting electrode can only be achieved for relatively thin (100 nm) P3HT/PCBM layers. Corresponding devices absorb only a limited fraction of all available photons but have the highest efficiency.

Introduction

Organic bulk-heterojunction (BHJ) solar cells made of blends of conjugated polymers as electron donors and functionalized fullerenes as electron acceptors have evolved as promising cost-effective alternatives to conventional inorganic photovoltaic devices.[1] In a typical organic solar cell, light absorption creates strongly bound excitons, which can dissociate into free charges only at donor/acceptor interfaces by rapid electron transfer from the donor to the acceptor.[2,3] Since the exciton diffusion length is limited to ~10 nm,[4] it is desirable for higher efficiency of BHJ cells that the donor and acceptor materials are well intermixed by forming phases in a nanometer range so that the donor/acceptor interface was maximized within the whole volume of a photoactive layer.

Once formed upon exciton dissociation, free holes and electrons should be transported through the donor and acceptor phases toward the corresponding electrodes; i.e., the (nanoscale) phases of donor and acceptor should form continuous percolation pathways leading to the positive and negative electrode, respectively. The transport of charge carriers can be enhanced if donor and/or acceptor (ideally both) are characterized by high mesoscopic order and crystallinity.[5] In addition, collection of charges can be facilitated in case where there is enrichment of the acceptor material at the side of the photoactive layer close to a negative (metal) electrode and enrichment of the donor material close to a positive electrode.[6,7] Such favorable concentration gradients of donor and acceptor materials through the thickness of the active layer ensure the existence of the shortest percolation paths to both electrodes and thus limit possibilities for charge recombination.

The external quantum efficiency η_{EQE} of a photovoltaic cell based on exciton dissociation at a donor/acceptor interface is $\eta_{EQE} = \eta_A \eta_{ED} \eta_{CC}$,[8] with the light absorption efficiency η_A, the exciton diffusion efficiency η_{ED}, which is a fraction of photogenerated excitons that reach a donor/acceptor interface before decaying, and the carrier collection efficiency η_{CC}, which is the probability that a free carrier generated at a donor/acceptor interface by dissociation of an exciton reaches its corresponding electrode. Thus, the efficiency of a BHJ is, besides the chemical architecture of the components applied, largely dependent on the light absorption efficiency *and* the local nanoscale organization of the photoactive layer in all three dimensions (Table 1). In particular, both the processing conditions of donor/acceptor mixtures from solution and the postproduction treatment like thermal annealing have a large influence on the performance of BHJ solar cells because they strongly affect the morphology, eventual crystalline order, and phase separation of the photoactive layer.[6,9−13]

Currently, one of the most promising BHJ systems, in terms of both efficiency and long-term stability, is the system based on regioregular poly(3-hexylthiophene) (P3HT) as the electron donor and the fullerene derivative [6,6]-phenyl-C_{61}-butyric acid methyl ester (PCBM) as the electron acceptor. The best performance is observed in P3HT/PCBM solar cells subjected to an annealing treatment, either at elevated temperature or during slow solvent evaporation, with the highest reported power conversion efficiencies of up to 5%.[10,14,15] Recently, the critical

*Corresponding author. E-mail: j.loos@tue.nl.

 Published on Web 09/10/2009

Table 1. Molecular and Morphology Requirements for the Photoactive Layer of a High-Performance Organic Solar Cell

	influenced by	
requirement	molecular architecture	morphology
absorption of incident light	levels of band gap(s)	thickness of the photoactive layer; roughness of interfaces
exciton dissociation	levels of the valence and conduction bands of the donor and acceptor materials	maximized interface: phases of the donor and acceptor in a range of ~10 nm (exciton diffusion length)
charge transport and collection	high mobility of free charge carriers	short and continuous percolation pathways leading through the donor phase to the positive electrode and through the acceptor phase to the negative electrode; high mesoscopic order and crystallinity of (ideally both) donor and acceptor; enrichment of donor close to the positive electrode and enrichment of acceptor close to the negative electrode
processability	optimized molecular architecture: stereoregiolarity, molecular weight (distribution), branching	thermodynamics and kinetics of film formation and phase separation

morphology parameters contributing to the improved performance of annealed P3HT/PCBM devices were identified by using the technique of electron tomography, which allows to image structures in three dimensions with nanometer resolution. It was shown that high performance after annealing goes hand in hand with favorable 3D morphological organization in P3HT/PCBM photoactive layers: formation of genuine 3D nanoscale networks with high crystalline order and favorable concentration gradients of both P3HT and PCBM through the thickness of the photoactive layer.[6]

The easiest and most straightforward way to get highly efficient organic BHJ cells would be to use sufficiently thick photoactive layers, in order to absorb as many photons as possible. In case of the P3HT/PCBM system, ~300 nm thick layers absorb most of the light. However, the best performance of P3HT/PCBM devices is often observed for thicknesses of active layers which are (up to 2 times) lower than those required for maximum light absorption.[14−16] The exact value of this optimum thickness for highest efficiency depends in general on many different parameters, such as chemical architecture of the components (viz. molecular weight distribution and regioregularity of P3HT), eventual, however minor, impurities in P3HT and/or PCBM (which may deteriorate electronic properties but may also promote crystal growth by serving as nucleation centers for crystallization), and exact processing condition, viz. type of the organic solvent used, presence of crystalline aggregates of P3HT or PCBM in solution/dispersion prior to film deposition, type of a film deposition technique used (spin-coating, doctor blading, inkjet printing), exact conditions of film formation (such as spin speed), etc. Also, the optimum layer thickness depends on the interference effects present in the thin film multilayer device[17] and can be influenced by the use of optical spacers.[18,19]

In this study, we focus on the relationship between, on one hand, device performance and, on the other hand, three-dimensional (3D) morphology of photoactive layers of different thickness in P3HT/PCBM bulk-heterojunction solar cells, both before and after thermal annealing. Our aim is to identify the reasons of poor performance in case of thicker photoactive layers absorbing more light but failing to convert it into more electricity. P3HT/PCBM photoactive layers of different thickness were obtained by varying the total concentration in solution and keeping the same all the preparation conditions (like the solvent used, spin speed, annealing time, and temperature). P3HT/PCBM layers with thickness of 50, 100, and 200 nm have been taken for this study, as layers having clearly different absorption levels (also when interference effects are taken into account)[17] and giving rise to distinctly different device performance. For a comprehensive morphology characterization of P3HT/PCBM layers, atomic force microscopy (AFM), electron diffraction, and the technique of electron tomography (or transmission electron microtomography) were applied; more information on the latter can be found in recent review publications.[20−23]

Experimental Section

Device Fabrication. P3HT (with M_n = 19 400 and PDI = 1.4 as determined by SEC, and regioregularity of 98% as determined by NMR, from Plextronics, Inc.) and PCBM (with purity of >99%, Solenne B.V.) were used as received. Mixed solutions were prepared by dissolving both components simultaneously in 1,2-dichlorobenzene (ODCB) in a 1:1 ratio, with total concentration ranging from 10 up to 34 mg/mL, and by stirring at room temperature overnight in the dark. It resulted in homogeneous solutions/dispersions with some P3HT aggregates present (as confirmed by UV−vis spectroscopy and TEM studies). The solutions were not filtered. The solar cell devices were fabricated by spin-coating a solution of P3HT and PCBM, sandwiched between a transparent anode and a cathode. The anode consisted of cleaned indium tin oxide (ITO) patterned glass substrates (Philips Research) covered by spin-coating a poly(3,4-ethylenedioxythiophene)/poly(styrenesulfonate) (PEDOT:PSS) dispersion (Baytron P VP AI 4083; H.C. Starck) after filtration using a 0.45 μm filter. The thickness of the PEDOT:PSS layer was around 70 nm as determined with a Tencor P-10 surface profiler. The cathode consisted of LiF (1 nm) capped with Al (100 nm).

The ITO-coated glass substrates were cleaned by ultrasonic treatment in acetone, followed by rubbing with soap, rinsing in dematerialized water, and refluxing in isopropyl alcohol to remove water, and finally they were treated in a UV-ozone oven for ca. 30 min.

Spin-coating (in air) of a P3HT/PCBM solution in ODCB on top of a PEDOT:PSS layer with a spin speed of 500 rpm for at least 4 min resulted in formation of homogeneous layers with thickness between 50 and 200 nm, depending on the total concentration in solution. After spin-coating, the samples were transferred into a glovebox with a nitrogen atmosphere to evaporate LiF and Al at pressure of 9×10^{-6} mbar. The active device area was 16.2 mm^2. Thermal annealing was performed on complete devices at 130 °C for 20 min on top of a hot plate inside a glovebox. Neither annealing for longer times (up to 1 h) nor annealing at different temperatures resulted in better devices than those reported here. Thicknesses of the photoactive layers were determined with a Tencor P-10 surface profiler.

Current−voltage characteristics were measured with a Keithley 2400 source measurement unit. Illumination was carried out with UV (GG 385) and infrared (KG1) filtered light from an uncalibrated tungsten halogen lamp (75 mW/cm^2). The light intensity of this light source provides for P3HT:PCBM blends a power output that is within 20% of the AM1.5 (100 mW/cm^2) performance.

Table 2. Performance and Morphological Parameters of Some of the P3HT/PCBM Solar Cells Used in This Study[a]

photoactive layer thickness (nm)	preparation conditions[b]	I_{sc} (mA/cm^2)	V_{oc} (V)	FF	η (%)	P3HT gradient[c]	overall P3HT crystallinity (%)
50	as spin-coated	2.6	0.55	0.60	0.8	N/A	23 ± 5[d]
50	annealed	3.4	0.58	0.58	1.2	yes (weak)	47 ± 3
100	as spin-coated	6.6	0.56	0.52	1.9	N/A	19 ± 5[d]
100	annealed	9.4	0.60	0.62	3.5	yes (strong)	55 ± 3
200	as spin-coated	5.5	0.53	0.56	1.6	no	30 ± 5
200	annealed	5.6	0.57	0.61	1.9	no	40 ± 3

[a] Short-circuit current density J_{sc}, open-circuit voltage V_{oc}, fill factor FF, power conversion efficiency η (not corrected for spectral mismatch), existence of P3HT gradient and degree of P3HT crystallinity. The structure of solar cells is in all cases ITO/PEDOT:PSS (70 nm)/P3HT:PCBM (1:1)/LiF (1 nm)/Al (100 nm). [b] All photoactive layers were spin-coated at 500 rpm. Different layer thickness is a result of different total concentration of P3HT/PCBM (1/1) in a solvent (*o*-dichlorobenzene). Thermal annealing was performed at 130 °C for 20 min on a hot plate in a N_2 atmosphere. [c] P3HT gradient and P3HT crystallinity were determined directly from the electron tomography data, unless indicated otherwise. Two observed P3HT gradients ("yes") refer to a situation where density of P3HT nanowires is larger at the bottom of the film, i.e., close to the hole collecting electrode ("favorable gradient"); see Figure 5. [d] This quantification was done by using electron tomography data of the corresponding thermally annealed films and correcting them for the ratio between the P3HT electron diffraction peak intensities from Figure 2c,f.

Absorption data were acquired using a Perkin-Elmer UV−vis spectrometer Lambda 40.

Atomic force microscopy images were acquired using a Solver P47HT with NSG 11 tips (both NT-MDT Co., Moscow, Russia).

Transmission Electron Microscopy Measurements. For TEM investigation, the P3HT/PCBM layers were floated from the water-soluble PEDOT:PSS substrate onto the surface of demineralized water and picked up with 200-mesh copper TEM grids. Bright field TEM morphology observation, acquisition of tilt series for electron tomography, and acquisition of electron diffraction patterns were performed on a Technai G^2 20 TEM (FEI Co.) operated at 200 kV. All tilt series were obtained in an automatic fashion by using Xplore3D software, the alignment and reconstruction of the data series were performed by using Inspec3D (both FEI Co.), and visualization of the 3D reconstructed volume was done with Amira 4.1 (Mercury Computer Systems, Inc.).

The *d*-spacings of P3HT and PCBM were obtained from the electron diffraction patterns by using nanocrystalline gold specimen for calibration.

The tilt series were acquired in the bright-field mode after preexposure of a specimen to the electron beam for a few minutes (to minimize sample shrinkage during tilt series acquisition), in the tilting range from −70° to +70°, by using a Saxton scheme with an increment of 1.5° at 0° tilt. The alignment of tilt series was based on tracking of general features (by cross-correlation) followed by tilt axis alignment. The reconstruction method used was SIRT (simultaneous iterative reconstruction technique); 20 iterations were applied.

Results and Discussion

For the combination of materials and the preparation route used in this study, the best device performance was observed for thermally annealed P3HT/PCBM photoactive layers of a moderate thickness of around 100 nm. Going to thinner or thicker photoactive layers resulted in poorer device performance, even in spite of improved light absorption in case of the thicker layers (Table 2 and Figure 1). It is especially remarkable that the number of free charges extracted at the electrodes is quite low in case of thicker photoactive layers, as reflected in the values of the short-circuit current (J_{sc}). Obviously, a straightforward increase of the photoactive layer thickness by adjusting concentration in solution, as performed in this study, does not guarantee that an optimum morphological organization gets reproduced in thicker layers and thus does not automatically lead to higher efficiency of solar cell devices. In the following, we analyze the volume morphology in relation with the layer thickness and focus on the possible reasons for the lower efficiency of thicker layers that absorb more photons. P3HT/PCBM photoactive layers with thickness of 50, 100, and 200 nm have been taken for a detailed morphological study.

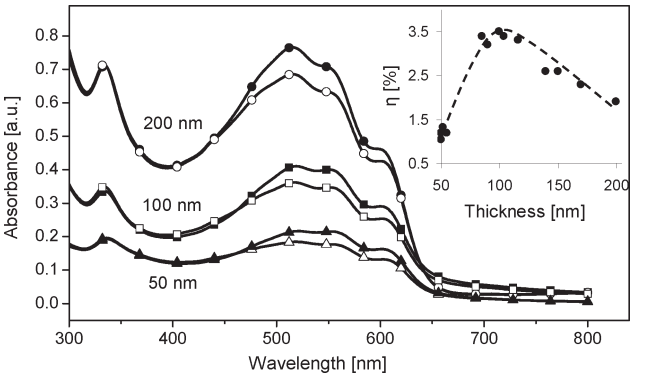

Figure 1. UV−vis spectra of P3HT/PCBM photoactive layers of different thickness (50−200 nm) giving rise to solar cell devices performing as listed in Table 2. Lines with open symbols correspond to layers directly after spin-coating and line with filled symbols to layers after subsequent thermal annealing. The inset shows a plot of the overall power conversion efficiency η (not corrected for spectral mismatch) of a number of thermally annealed devices as a function of the photoactive layer thickness. P3HT/PCBM photoactive layers with thickness of 50, 100, and 200 nm have been taken for a detailed morphological study.

Both P3HT and PCBM can crystallize: PCBM by eventually forming big bulky crystals (as often observed in blends of PCBM with amorphous poly(*p*-phenylenevinylene) MDMO-PPV)[24−26] and P3HT by forming crystalline nanowires with typical widths of around 15−25 nm, thickness of just a few nanometers, and lengths of hundreds of nanometers or even a few micrometers.[27] As mentioned in the Introduction, higher crystallinity of electron donor and acceptor materials enhances mobility of free charges (holes and electrons, respectively), which benefits device performance. The size and form of the crystals formed are however very critical: if the requirements of nanoscale phase separation and existence of percolating pathways leading to the electrodes are not met, higher crystallinity on its own will not lead to more efficient devices. For example, thermal annealing deteriorates the performance of MDMO-PPV/PCBM solar cells immediately as a result of formation of bulky PCBM crystals in the amorphous polymer-rich matrix (large-scale phase separation).[25,26] On the contrary, the shape of P3HT crystals is in general very suitable for high-efficiency bulk heterojunction: their width and thickness are in the right (nanometer) range to maximize the exciton dissociation at their interface with the second material of the photoactive layer, and their length makes them serve as efficient percolations throughout the BHJ.

It has been shown that the presence of crystalline P3HT nanowires suppresses formation of bulky PCBM crystals at any stage of P3HT/PCBM film formation (so that PCBM is present in the form of nanosized crystals only) and that improved crystallinity of P3HT after thermal annealing is one of the key factors

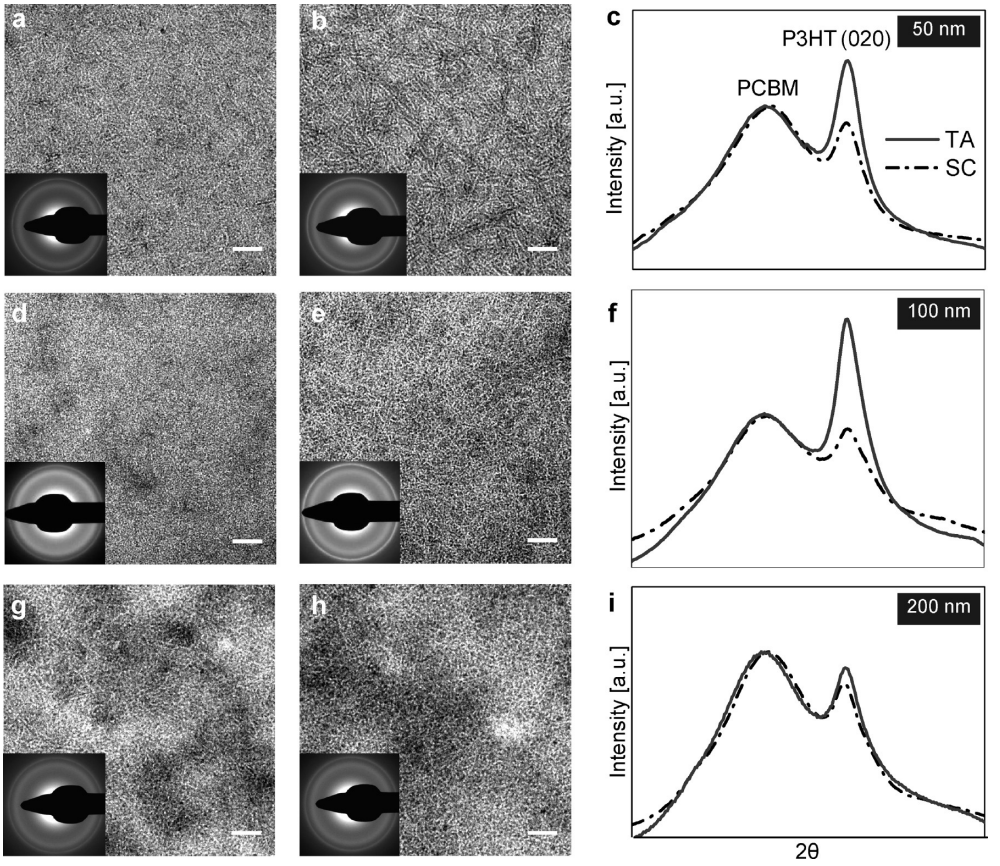

Figure 2. Bright-field TEM images of P3HT/PCBM photoactive layers with different thickness: 50 nm (a, b), 100 nm (d, e), and 200 nm thick (g, h). Images in (a), (d), and (g) correspond to layers obtained by spin-coating alone and images in (b), (e), and (h) to layers obtained after subsequent thermal annealing at 130 °C for 20 min. The scale bar is 200 nm. The insets are electron diffraction patterns acquired at the same spot as TEM images: a broad inner ring originates from PCBM nanocrystals (with *d*-spacing of 0.46 nm), and a thin outer ring comes from (020) reflections of P3HT crystals (*d*-spacing of 0.39 nm). The corresponding electron diffraction intensities were integrated all over the rings (besides the part masked by a beam stopper), normalized to the PCBM peak maximum and are plotted in (c), (f), and (i) as a function of the distance from the center of electron diffraction patterns, which scales with 2θ. TA refers to thermally annealed layers (solid line) and SC to spin-coated layers (dashed line).

accounting for improved efficiency of annealed P3HT/PCBM devices.[6,9,11,16] This was also the case with P3HT/PCBM photoactive layers used in this study. No bulky PCBM crystals were visualized by transmission electron microscopy (TEM), whereas crystalline P3HT nanowires can be distinguished in most TEM images as bright-looking fibrils (Figure 2). For bright-field TEM imaging, P3HT nanowires look bright and PCBM-rich regions dark because of the lower density of P3HT crystals (1.1 g/cm^3) as compared with PCBM (1.5 g/cm^3). Interpretation of such conventional TEM images can be quite complicated because these are essentially 2D projections of the actual 3D specimens under observation. Multiple stacking of the features which are relatively thin compared to the specimen's thickness, such as P3HT nanowires (a few nanometers thick) in the given P3HT/PCBM photoactive layers, will inevitably result in images looking blurred. Indeed, P3HT nanowires are most clearly visible in the thinnest (50 nm) films (Figure 2b). Further, the electron diffraction results show that P3HT crystallinity, characterized by the intensity of a bright outer Debye−Scherrer ring corresponding to (020) reflections,[27] increases after thermal annealing. This effect is especially pronounced in case of 50 and 100 nm thick films.

Corresponding atomic force microscopy (AFM) investigations of the photoactive layers morphology have also been performed. In contrast to TEM, AFM provides information on the morphology of the specimen's surface rather than on the internal film organization. As shown in Figure 3, the surface morphology is different in case of P3HT/PCBM photoactive layers of different thicknesses and before and after the thermal annealing treatment. Only in the 50 nm thin films are P3HT nanowires nicely visible on the top surface after thermal annealing (Figure 3b). In case of 100 nm or thicker P3HT/PCBM films (AFM images for thicker samples look similar to Figure 3d), no or only very few P3HT nanowires were detected by AFM, neither before nor after thermal annealing, even though P3HT is present in a (semi)-crystalline form in all these films, as shown by TEM imaging and electron diffraction results described above. The kinetics of P3HT film formation, phase separation in general, and crystallization during spin-coating and thermal annealing are different in case of films of different thickness. We assume that in thicker P3HT/PCBM layers amorphous, rather than crystalline, material is driven during crystallization to the top of the film.

To understand and to link the morphological organization and performance of photoactive layers of bulk heterojunction solar cells, it is essential to have information in terms of volume organization: how the morphology of a specimen looks like in all three dimensions, whether there are percolations to the top and bottom electrodes, etc. The technique that provides this volume information is electron tomography.[20−23]

Electron tomography is well-established to study biological structures, and recently, the first applications of this technique to photoactive layers of MDMO-PPV/PCBM and P3HT/PCBM have been reported.[6,12] This technique uses a series of 2D projections taken by TEM at different angles by tilting the specimen with respect to the electron beam in the TEM column. The series of 2D projections thus obtained is subsequently used to reconstruct a 3D image of the specimen on the basis of compu-

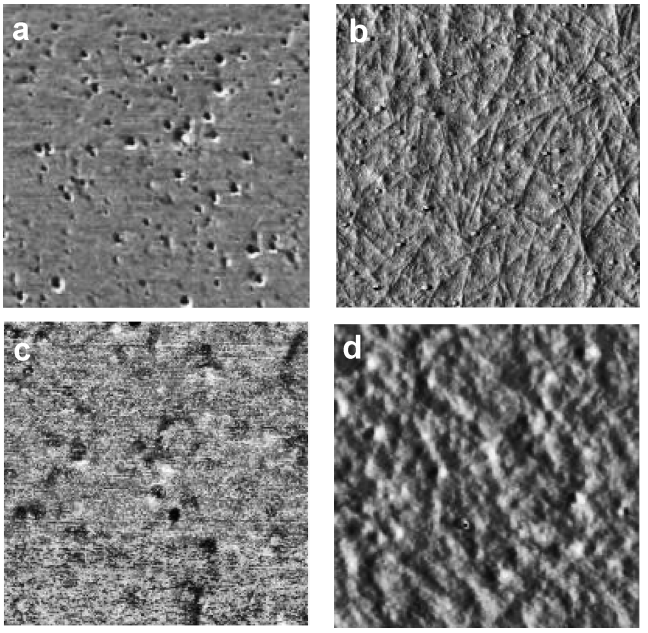

Figure 3. AFM phase images of P3HT/PCBM layers: 50 nm thick (a, b) and 100 nm thick (c, d). Layers in (a) and (c) were obtained by spin-coating only and in (b) and (d) by thermal annealing. Scan area is 2.5 μm × 2.5 μm.

terized tomography, with a nanometer-scale resolution. This 3D image can then be used, voxel by voxel, to study in detail the morphological organization.

The snapshots of the volume as obtained by electron tomography for some P3HT/PCBM layers used in this study are shown in Figure 4. In all presented volume data, crystalline P3HT nanowires are inclined in the volume of the film, signifying that P3HT forms genuine 3D rather than 2D networks. Such an existence of truly 3D networks of P3HT is beneficial for hole transport from any place within the photoactive layer to the hole collecting (positive) electrode.

Thinner films, 50 and 100 nm thick, that were obtained by spin-coating only revealed little features in the reconstructed volume (data not shown). The contrast between P3HT and PCBM is quite poor in these layers, which means that P3HT crystals are very imperfect: short and full of stacking defects. Low crystallinity of P3HT in these films is supported by electron diffraction data, too (Figure 2). After thermal annealing, crystallinity of P3HT in these layers (50 and 100 nm thick) increases dramatically, resulting in long perfect P3HT nanowires that were nicely visualized by electron tomography, as can be seen in Figure 4. The fact that these nanowires are indeed crystalline and not (partly) amorphous, has been additionally confirmed by conical dark-field TEM investigations (data no shown), where the image formation is governed by diffraction contrast as opposed to the mass−thickness and phase contrast in case of bright-field TEM.

Once volume data have been obtained, it is especially interesting to track possible morphology heterogeneities through the thickness of a P3HT/PCBM film (in *z*-direction), which can be done by dividing the reconstructed volume of a film into thin horizontal slices. Figure 4 shows few of such slices taken out of the volume data sets at different depths of P3HT/PCBM photoactive layers. It can be seen that in thermally annealed 50 and 100 nm films the density of P3HT nanowires is different on the bottom and on the top of the film, namely that the P3HT nanowires network is denser closer to the bottom, i.e., to the positive (PEDOT:PSS/ITO) electrode. This difference is especially strong in case of a thermally annealed 100 nm thick films. On the other hand, in 200 nm thick films, the distribution of crystalline P3HT nanowires is homogeneous through the film thickness. By going slice by slice through the reconstructed volume, the amount of crystalline P3HT nanowires can be quantified in relation to the actual *Z*-position within the photoactive layer (Figure 5).

Unlike crystalline P3HT nanowires, the rest of P3HT (in the amorphous form or in a form of small imperfect crystals) does not have sufficient contrast with PCBM and can hardly be visualized. However, it is most likely that (most of) the amorphous P3HT is located around the highly crystalline nanowires, as is generally the case in chain-folded polymer crystals. Thus, vertical segregation of P3HT most probably applies to all P3HT, including amorphous parts. Additionally, for device performance, it is most relevant to know how the perfect crystalline nanowires are distributed in the volume of the photoactive layer, rather than all P3HT: nanowires form a network of perfect "high-ways" for hole transport and thus largely determine the hole transport efficiency. The distribution of amorphous P3HT (best compared here to narrow slow country roads) is of less interest in this respect. The situation when more of the crystalline P3HT is located in the lower part of the film and more of PCBM in the upper part should be beneficial for collection of electrons and holes at the corresponding electrodes.[7]

In case of 200 nm thick P3HT/PCBM films, the morphological organization and trends in morphology development upon thermal annealing as revealed by electron tomography are different in few important aspects from thinner films. First, P3HT nanowires can already be distinguished in the 200 nm films right after spin-coating (Figure 4). The second difference is that there is no vertical segregation of (crystalline) P3HT in 200 nm films: the density of P3HT nanowires is basically the same in slices taken close to the bottom and to the top of the volume stacks, both in spin-coated and in annealed films. And finally, crystallization during film formation (spin-coating) as well as during the annealing treatment seems to follow different routes: initial crystallinity in the as spin-coated layer is already high, and only a small increase is observed after annealing (see Table 2).

Since it takes longer for a solvent to evaporate in these thicker films, P3HT crystallizes to a larger extent already during spin-coating. P3HT macromolecules retain their high mobility for longer time due to longer presence of the solvent in the film, and the resulting crystal organization is thus closer to the equilibrium state. Subsequent thermal annealing only slightly improves the quality of these P3HT crystals: the P3HT peak intensity in electron diffraction patterns increases somewhat (Figure 2i), and the P3HT nanowires get more pronounced (have higher contrast with PCBM-rich surroundings) in slices taken from the reconstructed volume stacks of thermally annealed films (Figure 4). Further, vertical segregation of crystalline P3HT or the absence thereof is also affected by the kinetics of film formation in P3HT/PCBM films of different thickness due to different solution viscosity and time it takes for a solvent to evaporate as this affects the nucleation behavior and (nano)crystal growth. Also, local solvent concentration differences in *z*-direction of the thicker layers may force precipitation of P3HT, which has now more time to crystallize. Subsequent annealing only results in healing of the crystal defects but not in substantial formation of additional crystals.

Recent studies of vertical composition in P3HT/PCBM films involved modeling of data obtained by variable-angle spectroscopic ellipsometry (VASE)[28] and the use of X-ray photoelectron spectroscopy (XPS) to compare composition of the bottom and top few nanometers of the films.[29] It concerned the total amount of P3HT and PCBM, without distinction between crystalline and amorphous P3HT. In both studies, it was stated that PCBM was preferentially concentrated on the bottom of the P3HT/PCBM films and P3HT closer to the top of the films and that the reason

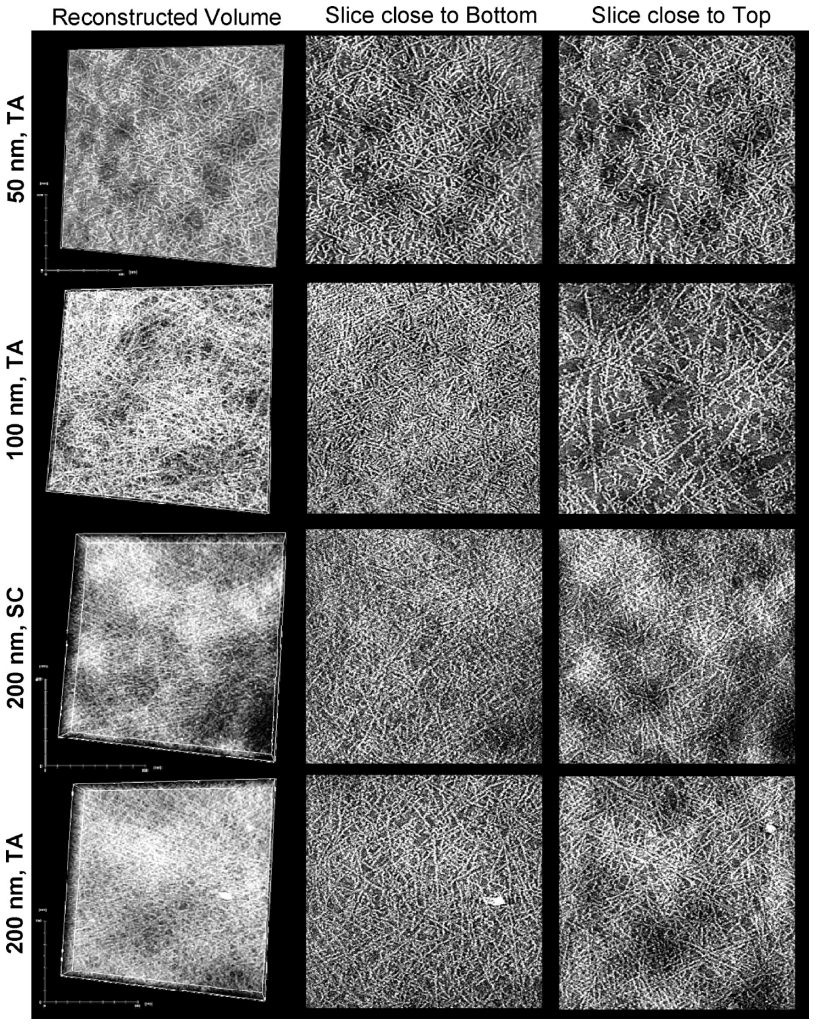

Figure 4. Results of electron tomography applied to P3HT/PCBM photoactive layers: thermally annealed (TA) 50 nm thick, thermally annealed 100 nm thick, as spin-coated (SC) 200 nm thick, and thermally annealed 200 nm thick layer. The first column represents snapshots of the corresponding film's whole reconstructed volume, and the second and third columns contain slices taken out of these 3D stacks: one slice close to the bottom of the film (i.e., next to PEDOT:PSS layer) and another slice close to the top of the film (i.e., LiF/Al electrode). The dimensions of the slices, or lateral dimensions of the 3D volume, are around 1700 nm × 1700 nm.

for this is high surface energy of the PEDOT:PSS layer. There are also SIMS (secondary ion mass spectrometry) studies of MDMO-PPV/PCBM[30] and polyfluorene/PCBM blends,[31] which show homogeneous distribution of both polymer and PCBM through the film thickness.

The advantage of the use of electron tomography to study vertical organization in P3HT/PCBM films is that it allows direct observation of the morphology of crystalline P3HT nanowires with high accuracy at any depth of the film, without any intermediate steps of modeling (requiring as an input some assumptions on morphological organization[28]) and without the risk of introducing artifacts, such as carbon and oxygen contaminations in the case of surface-sensitive XPS.[29]

Unlike previous studies, we have observed two types of vertical organization in P3HT/PCBM films depending on the film preparation and resulting film thickness: (1) enrichment in crystalline P3HT nanowires in the lower part of the films (in case of 50 and 100 nm thick annealed P3HT/PCBM layers) and (2) homogeneous distribution of crystalline P3HT through the film thickness (in 200 nm thick layers). As outlined above, it is most probable that this vertical organization applies to all P3HT. These different types of vertical organization in the P3HT/PCBM films of different thickness deposited on the same PEDOT:PSS substrate dismiss the key role of the underlying substrate's surface energy for formation of vertical gradients.

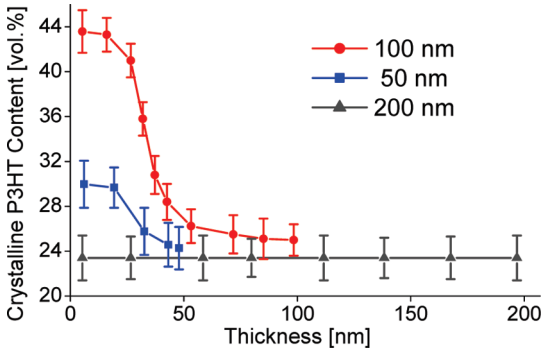

Figure 5. Quantification of the crystalline P3HT nanowires distribution through the thickness of the thermally annealed (TA) P3HT/PCBM photoactive layers: 50, 100, and 200 nm thick. The thickness of 0 nm corresponds to the bottom side of the layer, i.e., the one next to the hole collecting PEDOT:PSS/ITO electrode.

On the basis of the electron tomography data, such as plots presented in Figure 5, the overall crystallinity of P3HT in the P3HT/PCBM photoactive layers can be straightforwardly quantified.[6] Since

hole transport is a limiting factor in P3HT/PCBM device performance, higher P3HT crystallinity (hence higher hole mobility[32,33]) combined with more favorable morphological organization with improved connectivity (pathways) leading to the hole-collecting electrode result in general in more efficient solar cell devices. This trend holds in the given P3HT/PCBM films, too (see Table 2).

However, the levels of P3HT crystallinity cannot explain all the differences observed in this study; namely, they cannot explain a relatively poor performance of (both) 200 nm thick films and of 50 nm thermally annealed P3HT/PCBM films. If we consider the scale of phase separation, it is hardly different in all the films and cannot be the primary reason for it. One might even say that the PCBM-rich domains are the largest, and larger than desirable, in the top half of the 100 nm thermally annealed films, which actually show the best performance. From the data presented in Table 2 and in Figure 5, it follows that, along with a high level of the overall P3HT crystallinity in a photoactive layer, high density of P3HT nanowires close to the bottom hole collecting electrode and correspondingly enrichment of PCBM in the top part of the film are critical for high device performance. These favorable concentration gradients of donor and acceptor materials through the thickness of the active layer ensure existence of the shortest percolation paths to both electrodes and thus limit possibilities for charge recombination.

An additional reason for a poorer performance of 50 nm thick thermally annealed films lies very probably in the fact that in these films the P3HT nanowires are located on the top surface, as shown by AFM (Figure 3), too. This was not observed in any other P3HT/PCBM films in this study: no other films had crystalline P3HT nanowires directly on the top surface. AFM is in this sense complementary to the data obtained by electron tomography, which often cannot provide reliable information on morphology of the very bottom and top part of a film (the first and last ~2 nm). The presence of crystalline P3HT nanowires (hole transporters) on the top surface (right next to the electron collecting electrode) may be the very reason for a decrease in fill factor (FF) upon annealing in 50 nm films (whereas FF increases after annealing in thicker layers) and for relatively low J_{sc} values: less than a half of J_{sc} observed in 100 nm thick films.

Conclusions

In this study, we looked at the relationship between device performance and 3D morphology of photoactive layers of different thickness in P3HT/PCBM bulk-heterojunction solar cells, before and after thermal annealing. The morphology of polymer (-based) films is in general strongly dependent on the film preparation process. Here, we minimized the differences in P3HT/PCBM films preparation by varying the total concentration in solution (hence solution viscosity and final film thickness) and keeping the same all the other parameters (like the solvent used, spin speed, annealing time, and temperature).

The changes after thermal annealing in the films of the same thickness were observed to be largely the same as previously reported: improved power conversion efficiency after annealing was a result of improved crystallinity of P3HT forming genuine 3D networks with favorable concentration gradients of crystalline P3HT and PCBM through the thickness of the photoactive layer. This effect was, however, marginal in case of thicker (200 nm) P3HT/PCBM films: both P3HT crystallinity and device performance improved only slightly after thermal annealing, while no concentration gradients were observed.

If we compare thermally annealed P3HT/PCBM films of different thickness with each other, the basic conclusion is that an optimum morphological organization of a photoactive layer in all three dimensions is more crucial for high efficiency of solar cell devices than absorption alone. The best device performance was obtained using moderately thick (100 nm) P3HT/PCBM photoactive layers characterized by high overall crystallinity of P3HT, namely more numerous and more perfect crystalline P3HT nanowires forming a genuine 3D network, and by enrichment of P3HT close to the hole collecting electrode (and, correspondingly, enrichment of PCBM close to the electron collecting electrode). Thicker films (200 nm thick) absorb more light but show less favorable morphological organization in photoactive layers (lower crystallinity of P3HT, especially next to the hole collecting electrode) and as a result produce poorly functioning solar cell devices.

Different types of vertical organization in the P3HT/PCBM films of different thickness deposited on the same PEDOT:PSS substrate dismiss the key role of the underlying substrate's surface energy for formation of vertical gradients, as suggested by previous studies. On the basis of the findings of this study, we can conclude that the existence and type of composition gradients through the thickness of the active layer are largely determined by the kinetic aspects of film formation due to different solution viscosity, different time it takes for the solvent to evaporate, and eventual differences in local solvent concentration. These aspects have a direct impact on how long the (macro)molecules are mobile in the given solution/dispersion, on eventual precipitation of components depending on local variations in solvent concentration, and thus on formation of nuclei and subsequent growth and distribution of (nano)crystals throughout the active layer.

To sum up, a straightforward increase of a photoactive layer thickness by adjusting the total concentration in solution does not guarantee that optimum morphological organization gets reproduced in thicker layers and does not automatically lead to higher efficiency of thicker solar cell devices, even though they effectively absorb more light. Different aspects of the kinetics of film formation and crystallization influence the final 3D morphological organization in films of different thickness and, correspondingly, performance of the solar cell devices.

Acknowledgment. The financial support was provided by the Dutch Polymer Institute (project No. 524). The authors also thank Erik Nies and Peter Thüne for fruitful discussions.

References and Notes

(1) Mayer, A. C.; Scully, S. R.; Hardin, B. E.; Rowell, M. W.; McGehee, M. D. *Mater. Today* **2007**, *10*, 28.
(2) Sariciftci, N. S.; Smilowitz, L.; Heeger, A. J.; Wudl, F. *Science* **1992**, *258*, 1474.
(3) Haugeneder, A. *Phys. Rev. B* **1999**, *59*, 15346.
(4) Shaw, P. E.; Ruseckas, A.; Samuel, I. D. W. *Adv. Mater.* **2008**, *20*, 3516.
(5) Sirringhaus, H. *Nature* **1999**, *401*, 685.
(6) Van Bavel, S. S.; Sourty, E.; De With, G.; Loos, J. *Nano Lett.* **2009**, *9*, 507.
(7) Kumar, A.; Li, G.; Hong, Z.; Yang, Y. *Nanotechnology* **2009**, *20*, 165202.
(8) Peumans, P.; Yakimov, A.; Forrest, S. R. *J. Appl. Phys.* **2003**, *93*, 3693.
(9) Yang, X.; Loos, J.; Veenstra, S. C.; Verhees, W. J. H.; Wienk, M. M.; Kroon, J. M.; Michels, M. A. J.; Janssen, R. A. J. *Nano Lett.* **2005**, *5*, 579.
(10) Li, G.; Shrotriya, V.; Huang, J.; Yao, Y.; Moriarty, T.; Emery, K.; Yang, Y. *Nat. Mater.* **2005**, *4*, 864.
(11) Hoppe, H.; Sariciftci, N. S. *J. Mater. Chem.* **2006**, *16*, 45.
(12) Yang, X.; Loos, J. *Macromolecules* **2007**, *40*, 1353.
(13) Peet, J.; Kim, J. Y.; Coates, N. E.; Ma, W. L.; Moses, D.; Heeger, A. J.; Bazan, G. C. *Nat. Mater.* **2007**, *6*, 497.
(14) Reyes-Reyes, M.; Kim, K.; Carroll, D. *Appl. Phys. Lett.* **2005**, *87*, 083506.
(15) Ma, W.; Yang, C.; Gong, X.; Lee, K.; Heeger, A. J. *Adv. Funct. Mater.* **2005**, *15*, 1617.
(16) Padinger, F.; Rittberger, R. S.; Sariciftci, N. S. *Adv. Funct. Mater.* **2003**, *13*, 85.
(17) Hoppe, H.; Shokhovets, S.; Gobsch, G. *Phys. Status Solidi RRL* **2007**, *1*, R40.

(18) Hansel, H.; Zettl, H.; Krausch, G.; Kissilev, R.; Thelakkat, M.; Schmidt, H.-W. *Adv. Mater.* **2003**, *15*, 2056.
(19) Gilot, J.; Barbu, I.; Wienk, M. M.; Janssen, R. A. J. *Appl. Phys. Lett.* **2007**, *91*, 113520.
(20) Jinnai, H.; Spontak, R. J. *Polymer* **2009**, *50*, 1067.
(21) Weyland, M.; Midgley, P. A. *Mater. Today* **2004**, *7*, 32.
(22) Möbus, G.; Inkson, B. J. *Mater. Today* **2007**, *10*, 18.
(23) Midgley, P. A.; Ward, E. P. W.; Hungria, A. B.; Meurig Thomas, J. *Chem. Soc. Rev.* **2007**, *36*, 1477.
(24) Yang, X.; Van Duren, J. K. J.; Rispens, M. T.; Hummelen J. C.; Janssen, R. A. J.; Michels, M. A. J.; Loos, J. *Adv. Mater.* **2004**, *16*, 802.
(25) Hoppe, H.; Niggemann, M.; Winder, C.; Kraut, J.; Hiesgen, R.; Hinsch, A.; Meissner, D.; Sariciftci, N. S. *Adv. Funct. Mater.* **2004**, *14*, 1005.
(26) Yang, X.; Van Duren, J. K. J.; Janssen, R. A. J.; Michels, M. A. J.; Loos, J. *Macromolecules* **2004**, *37*, 2151.
(27) Ihn, K. J.; Moulton, J.; Smith, P. *J. Polym. Sci., Part B: Polym. Phys.* **1993**, *31*, 735.
(28) Campoy-Quiles, M.; Ferenczi, T.; Agostinelli, T.; Etchegoin, P. G.; Kim, Y.; Anthopoulos, T. D.; Stavrinou, P. N.; Bradley, D. D. C.; Nelson, J. *Nat. Mater.* **2008**, *7*, 158.
(29) Xu, Z.; Chen, L.-M.; Yang, G.; Huang, C.-H.; Hou, J.; Wu, Y.; Li, G.; Hsu, C.-S.; Yang, Y. *Adv. Funct. Mater.* **2009**, *19*, 1227.
(30) Van Duren, J. K. J.; Yang, X.; Loos, J.; Bulle-Lieuwma, C. W. T.; Sieval, A. B.; Hummelen, J. C.; Janssen, R. A. J. *Adv. Funct. Mater.* **2004**, *14*, 425.
(31) Nilsson, S.; Bernasik, A.; Budkowski, A.; Moons, E. *Macromolecules* **2007**, *40*, 8291.
(32) Mihailetchi, V. D.; Xie, H.; De Boer, B.; Koster, L. J. A.; Blom, P. W. M. *Adv. Funct. Mater.* **2006**, *16*, 699.
(33) Vanlaeke, P.; Swinnen, A.; Haeldermans, I.; Vanhoyland, G.; Aernouts, T.; Cheyns, D.; Deibel, C.; D'Haen, J.; Heremans, P.; Poortmans, J.; Manca, J. V. *Sol. Energy Mater. Sol. Cells* **2006**, *90*, 2150.